

Hydrological characteristics of Chernobyl catchment: assessment of catchment scale long-term water balance and future situation

Yasunori Igarashi¹, Mark Zheleznyak¹, Hlib Lisovyi², Yoshifumi Wakiyama¹, Yuichi Onda³, Kenji Nanba¹, Alexei Konoplev¹, Gennady Laptev², Dmitry Samoilo⁴, and Serhii Kirieiev⁴

¹Fukushima University

²Ukrainian Hydrometeorological Institute

³University of Tsukuba

⁴Chernobyl Ecocentre

May 5, 2020

Abstract

Changes in the catchment scale water balance have important social implications for usable water now and in the future. Stream discharge is also directly related to radionuclides flux in the river water system. The aim of this study was to clarify the water balance in the Chernobyl Exclusion Zone (CEZ) under current and future climate conditions. A catchment scale hydrological model was used with long-term discharge data to project the future trend of radionuclides wash-off from the contaminated catchment at the CEZ in Ukraine. The Sakhan river catchment at the CEZ (51.41°N, 30.00°E) in Ukraine is one of the Pripyat river systems, and has a total surface area of 186.9 km². We found that under the current climate, 84% of annual input (sum of rainfall and snowmelt) was consumed as evapotranspiration, and discharge was estimated to be 16%. In future climates, annual precipitation is expected to increase. However, a projected increase in the vapor pressure deficit led the consumption of precipitation as evapotranspiration and no significant increase in discharge. The study found that warmer winter and spring temperatures will decrease the snowfall, and increase the rainfall, but it was not enough to increase evapotranspiration. As a result, the peak of discharge shifted from April to March. The increase of future average discharge during the winter and spring came from a combination of (1) increasing rainfall in the winter and spring, and (2) relatively small levels of evapotranspiration, which enhanced the catchment scale water recharge in soil moisture and gave rise to greater discharge during winter and spring. The reduction of extreme river discharge from the hydrological projections could reduce the probability of high radionuclides concentration in the river water system in the future, owing to the reduction of surface runoff water from the contaminated surface soil and/or top layer of floodplain soils in the CEZ.

Introduction

After the Chernobyl nuclear power plant (CNPP) accident in April 1986, the Chernobyl Exclusion Zone (CEZ) has become known as one of the most radionuclide-contaminated terrestrial ecosystems on Earth (UNSCEAR, 2000; IAEA, 2006; Nepyivoda, 2005). Even now, the redistribution of long-lived radionuclides, such as ¹³⁷Cs and ⁹⁰Sr, from the contaminated area has been of great concern in terms of the radiological risks for residents in the downstream area (e.g., Smith et al., 2005; IAEA, 2006). River water discharge is directly related to radionuclides flux in the river water system because dissolved and particulate radionuclide transportation mechanisms, which are associated with water movement and sediment transport, are important processes of radionuclides redistribution (e.g., Garcia-Sanchez and Konoplev, 2009; Yoshimura et al., 2015; Wakiyama et al., 2019). Understanding the characteristics of the catchment scale water balance, including discharge (Q), precipitation (P_r), and evapotranspiration, in the CEZ and showing how these

could change in future climates is critical for the radionuclide redistribution from CEZ as well as water resources downstream.

Over annual and longer time scales, an approximate balance exists between groundwater inflow and outflow, and the difference between P_r and Q must be balanced by E (e.g., Brutsaert, 1982; Palmroth et al., 2010). Changes in the catchment scale water balance, due to the changes in P_r and/or E trend, have important social implications for the amount of usable water now and in the future (e.g., Foley et al., 2005). The catchment scale water balance is also closely connected with the transport of dissolved ions and the radionuclides flux (e.g., Garcia-Sanchez et al., 2005; Tsuji et al., 2016; Egusa et al., 2019). The water balance in northern Ukraine had been studied from a climatological aspect because of its importance for agriculture. Annual E , which can be estimated from P_r and solar radiation, used most of the P_r (Budyko, 1961). Even on a global scale, it is widely known that most P_r is consumed as E , when P_r is low (Zhang et al., 2001). For instance, Zhang's equation indicates that 80%–90% of P_r could make up E when precipitation was assumed to be 600 mm/year. Thus, E is an important component of the regional water balance, especially for low P_r regions, such as northern Ukraine. It is considered that the future water balance in this region will be a critical issue. Many recent studies have been dedicated to future changes of climate in Europe. The climate projections under different emission scenarios show a temperature increase over Europe in the range of 1–4.5 °C under RCP4.5 and 2.5–5.5 °C under RCP8.5 by the end of the century (EEA, 2017). Annual precipitation totals show a less clear signal of change in the 21st century compared with temperature, although there is agreement from most projections on an overall annual increase in northern and eastern Europe (Jacob et al., 2014; Kjellström et al., 2011), with a rise in flood frequencies (Lehner et al., 2006). The future river discharge rate will increase due to the greater annual P_r in the Polish river network (Piniewski et al., 2018). Increasing river discharge is also projected with higher precipitation and air temperature at the Teteriv catchment in northern Ukraine (Didovets et al., 2017). However, changes in discharge rate are affected not only by changes in precipitation, but also by evapotranspiration, which is largely controlled by the vapor pressure deficit (combination of temperature and humidity). Climate change is projected to result in significant changes in the seasonality of river flows across Europe. Summer flows are projected to decrease over most of Europe, including in regions where annual flows are projected to increase. Where precipitation shifts from snow to rain, spring and summer peak flow will shift to earlier in the season (EEA, 2017).

At the catchment scale, over different time periods, the difference between P_r and Q must be balanced by E (Brutsaert, 1982). The water balance at long time scales can be simplified based on this steady state assumption of vegetation impact (e.g., Laio et al., 2001; Palmroth et al., 2010). As many previous studies have shown, catchment scale E is strongly controlled by the soil water content (W) and vapor pressure deficit (D) (e.g., Gollan et al., 1985; Kumagai et al., 2004; Igarashi et al., 2015b, 2015c). According to a simplified catchment scale water budget (Palmroth et al., 2010), P_r should be perfectly distributed into E , Q and W . This simplification could help to understand the hydrological characteristics and radionuclides dynamics at the CEZ, and to provide the first order approximation for a catchment scale water balance under current climate conditions. In addition, hydrological model simulation and projected climate allow us further discussion of hydrology situation and following radionuclides discharge in this region.

The purpose of this study was to clarify the water balance in a catchment in the CEZ climate. River discharge data covering over 25 years were used for the E modeling, which was controlled by D and W . Interestingly, these long-term data were collected for the monitoring of radionuclides wash-off in the CEZ. Bias-corrected future climate predictions from general circulation model (GCM) outputs were used for evaluating the hydrological water balance in the CEZ. We aimed to predict the future hydrological dynamics and to provide baseline information for future wildlife and ecosystem dynamics.

Material and Methods

Field measurements of river discharge

Experiments were conducted at the Sakhan River in the CEZ (51.41°N, 30.00°E) (Fig. 1). The Sakhan River lies within one of the sub-catchments of the Pripyat River system and has a total area of 186.9 km². The

catchment is largely covered by grass meadows and forest. There is a limited area of wetland. The forest contains both coniferous and mixed forests. Geological strata are composed of sandy quaternary deposits (Igarashi et al., submitted). The long-term stream discharge data used in this study were monitored for countermeasure of radionuclides concentrations and river water discharge from the small catchment to the larger river system. The data were measured approximately every 2 weeks by two research institutes, the Ukrainian Hydrometeorological Institute (data period: 1994–1998) and State Agency of Ukraine on Exclusion Zone Management and Chernobyl Ecocentre (data period: 1999–2018). The discharge rate was estimated by the existing height-discharge ($H - Q$) relationship equation at the outlet of the catchment. The H and Q were obtained by integrating the cross-sectional observation of the flow velocity and water depth, where the bed was contained by a concrete revetment under the bridge. To verify our estimates, flow rates were also measured directly using an electromagnetic current meter (VE20, KENEK, Japan) from March to May 2018, but differences in the results were insignificant. Therefore, the flow rate data used in this study were all derived from the Manning equation without correction. Observed Q are shown in Fig. 3e and f (e: logarithmic-scale and f: normal scale). Clear seasonality of Q was observed; Q began to increase from February, was high during the spring because of snow melt, and gradually decreased into summer. After the summer, Q started to increase again gradually. The maximum Q was observed in April 2013 (Fig. 2e and f).

Field measurement of climate variables

The long-term measurements of meteorological variables were obtained at the monitoring point of the Central Geo-survey Organization in Chernobyl (51°15'58.3"N, 30°13'32.9"E), in an open site 20 km away from the discharge monitoring point. Daily precipitation (P_r ; mm), daily mean temperature (T_a : degC), relative humidity (RH: %), and snow depth (S_d : cm) were calculated every 3 hours by a human observer with a self-made storage-type rain gauge, and dry-wet thermometer. Vapor pressure deficit (D) was calculated from the observed T_a and RH. During the 25-year observation period, annual precipitation was 604 ± 93 mm yr⁻¹ (mean ± S.D.) (Fig. 3a). The snow cover period is from November to March of the following year, but depending on the year, occasionally snow cover is observed in October or April/May (Fig. 3b). The average annual temperature was 8.3 ± 0.6 degC (Mean ± S.D.). The maximum and minimum daily T_a were 29.1 degC and -25.0 degC, respectively (Fig. 3c). The annual average D was 0.40 ± 0.04 kPa (Fig. 3d). D also had a distinct seasonality, with an average value of 0.79 kPa in July, peaking in winter and also high in summer (Fig. 3d). Q was highest during March during the snowmelt season. It decreased toward the summer (Fig. 3e and f). Precipitation increased in summer, but the decrease in summer flow was lower than in other seasons because evapotranspiration was higher, as a result of greater evaporation demand from the atmosphere from high summer D (Igarashi et al., submitted).

Models for current and future hydrological simulation

Hydrological model

The catchment water balance, over a given time period, is described as a simple dynamic system defined by a zero-dimensional model. The change in the watershed water storage W can be expressed as:

$$\frac{dW}{dt} = R_f + S_m - Q - E + Q_{in} - Q_{out} \approx R_f + S_m - Q - E(1)$$

The water storage (W : mm) in the entire watershed governs the runoff-storage relationship. At long time scales, the water balance reflects changes in W , stream discharge (Q : mm), evapotranspiration (E : mm), and inputs, which are rainfall (R_f : mm) and snowmelt (S_m : mm). We describe the details of R_f and S_m in section 3.2. Here, Q_{in} and Q_{out} are groundwater outflow and inflow, respectively, across the watershed boundaries. In this study, we used the following assumptions (Palmroth et al., 2010): (1) the net groundwater flow across the reservoir boundaries is zero ($Q_{in} - Q_{out} = 0$) and, hence, the only inflow of water is $R_f + S_m$ and the only outflows are E and Q ; (2) the saturated and unsaturated and/or shallow and deep storages are lumped in a single term (W); and (3) the entire water storage is accessible by the roots of the vegetation cover in the watershed.

The Q was assumed to be at its maximum for saturated soil moisture conditions. Q can be expressed using

the hydraulic conductivity model proposed by Brutsaert (1968):

$$Q = Q_o (\theta)^m \quad (2)$$

where Q_o is the maximum run-off flux parameter (mm d^{-1}) and m is the fitted parameter. $\theta (= W / W_{\max})$ is the soil moisture and degree of saturation varying between 0 and 1. W_{\max} is the maximum water depth.

As previous studies have shown, E is strongly controlled by the soil water content and D (e.g., Ewers et al., 2001; Pataki and Oren, 2003; Igarashi et al., 2015a, 2015b). In this model, the main limiting factors controlling evapotranspiration were considered to be s and D . Here a modified Laio's model (c.f., Laio et al. 2001; Manzonni et al., 2011) was used to compute evapotranspiration, given by:

$$E(\theta, t) = \begin{cases} 0, & \& 0 < \theta(t) \leq \theta_h \\ \alpha \left[E_w \frac{\theta(t) - \theta_h}{\theta_w - \theta_h} \right] D, & \& \theta_h < \theta(t) \leq \theta_w \\ \alpha \left[E_w + (E_{\max} - E_w) \frac{\theta(t) - \theta_w}{\theta^* - \theta_w} \right] D, & \& \theta_w < \theta(t) \leq \theta^* \\ \alpha E_{\max} D, & \& \theta^* < \theta(t) \leq 1 \end{cases} \quad (3)$$

where E_w and E_{\max} are the soil evaporation and the maximum evapotranspiration, respectively, and θ_h , θ_w and θ^* are s at 'hygroscopic point', 'plant wilting point' and 'plant stress point', respectively. When θ falls below a given θ^* , plant transpiration is reduced by stomatal closure to prevent internal water losses. Then, soil water availability becomes a key factor in determining the actual evapotranspiration rate. Transpiration and root uptake continue at a reduced rate until θ reaches θ_w . Below θ_w , soil water is further depleted only by evaporation at a low rate to θ_h . a is unit conversion factor (kPa^{-1}).

Snow model

Snow is the critical component of a snow-covered catchment during the winter. We calculated the snowfall and snowmelt by the water equivalent of snow.

$$\frac{dS}{dt} = S_f - S_m \quad (4)$$

$$R_f = P_r (1 - F) \quad (5)$$

$$S_f = P_r F \quad (6)$$

Here, S (mm) is the snow depth of water equivalent. S_f (mm) and S_m (mm) are water equivalent of snow fall and snowmelt, respectively. The rate of S_f and R_f (Eq. 1) are calculated by using the simple temperature-dependence model (Dai, 2008). F is the conditional snow frequency. As shown in Dai (2008), the F (%) - T_a ($^{\circ}\text{C}$) relationship has been well fitted with a hyperbolic tangent function as follows:

$$F(T_a) = a \{ \tanh [b(T_a - c)] d \} \quad (7)$$

Here, T_a is the air temperature, a , b , c , and d are the fitted parameters. In this study, we used the typical parameter set for terrestrial surfaces (Dai, 2008). Snowmelt is also calculated by using a simple model, called the "Degree-day method" (Hock, 2003) as follows:

$$S_m = \begin{cases} 0, & \& T_a < 0 \\ f_m T_a, & \& T_a \geq 0 \end{cases} \quad (8)$$

Here, f_m ($\text{mm } ^{\circ}\text{C}^{-1} \text{ day}^{-1}$) is the melting factor. We assumed that the air temperature equal to zero ($T_a = 0$) a threshold temperature beyond which melt is assumed to occur. f_m is estimated as $3.0 \text{ mm degC}^{-1} \text{ day}^{-1}$ from the snow depth record in Chernobyl. The list of parameters is shown in Table 1.

Model validation

The estimation of water and solute fluxes in the system requires the determination of the model parameters. The remaining parameters were estimated through a Markov Chain Monte Carlo (MCMC) calibration procedure using the Differential Evolution Adaptive Metropolis (DREAM) script in *R* (Vrugt et al., 2009; Joseph and Guillaume, 2013). These comprise five hydrologic parameters (Q_o , m , and W_{max} for the storage-discharge relationships, E_w , and E_{max} for evapotranspiration). All parameters were calibrated against daily discharge data over the 25-year period from 1994 to 2018. The model was run in daily time steps. The bi-weekly measurements may not capture all the high and low-frequency dynamics. However, the measurements ($n=649$) were collected during very different hydrologic conditions and they covered all seasons from high water levels during the snowmelt to low water levels during summer. After the model validation, the best fit parameters are obtained as Table 2. Nash-Sutcliffe coefficients (NSC: Nash and Sutcliffe, 1970) and R^2 were 0.62 and 0.79, respectively. In terms of evaluation, the classification suggested by Motovilov et al. (1999) was adopted, described as: $NSC > 0.75$ (model is appropriate and good); $0.36 < NSC < 0.75$ (model is satisfactory); and $NSC < 0.36$ (model is unsatisfactory). Thus, it is considered that the agreement of this model is appropriate as a first order approximation of the long-term water balance simulation. The model was able to simulate high Q during the snowmelt season in 2013 and 2018 (Fig. 3b), and the low Q period in 2002, 2003 and 2017 (Fig. 3c). It should be noted that the forested area has partly increased after the accident due to natural plant succession with no agricultural management (human pressure) in the CEZ (Yoschenko et al., 2019), and our model does not address the impact of long-term vegetation changes on evapotranspiration. However, we did not find clear differences in model agreement in the first and last 10-year periods. Thus, we used constant parameters for the model simulation.

Future hydrological simulation

To simulate catchment scale future water balance, the GCM output was used as the forcing data for our hydrological model (Eq. 1). In this study, MRI-CGCM3 (Yukimoto et al., 2012) was selected for our hydrological model because of the 1.125degx1.125deg high resolution with 4-types of Representative Concentration Pathways (RCP) scenarios (RCP8.5) as the forcing future climate. In this study, simple bias-correction was applied by adding (or multiplying) (e.g., the “delta method” (e.g., Graham et al., 2007; Sperna Weiland et al., 2010);

$$x_{cor, i} = x_{o, i} + \mu_p - \mu_b \quad (9)$$

$$x_{cor, i} = x_{o, i} \times \frac{\mu_p}{\mu_b} \quad (10)$$

where $x_{cor,i}$, $x_{o,i}$ denotes the bias-corrected data and observed data for each single day during the baseline period (13 years; from 2006 to 2018), respectively. The μ_b and μ_p indicate the averaged simulated data in the baseline period and projection period, respectively. Based on a previous study (Watanabe et al., 2012), equation (1) was used for T_a and D , and equation (2) was used for P_r .

Results and discussions

In this study, we created a model to estimate evapotranspiration from 25-year runoff and forcing meteorological factors. The model reproduced the observed values well. In the results, we will first show the water balance and the trend of each hydrological element over 25 years. Then, the water balance in a future climate will be illustrated.

Catchment scale long-term water balance and trends

Fig. 4 shows the relationship between the annual water input ($I_A = R_f + S_m$) and evapotranspiration and discharge. It should be noted that when evapotranspiration exceeds the annual input here the previous year’s storage water is carried over to the next year due to the snow and soil water content. The 25-year (from 1994 to 2018) averaged I_A at this study catchment was estimated as 604 ± 93 (mm), while the E was 507 ± 50 (mm) and Q was 102 ± 50 (mm) (Table 3). We found that the 84% of rainfall was consumed as evapotranspiration, and river flow was 16%. As shown in Zhang et al. (2001), if annual precipitation is approximately 600 mm, the proportion of evapotranspiration against annual input is very high. We also found a clear response of E and Q to I_A (Fig. 4). Zhang et al. (2001) estimated the evapotranspiration range

from observations under various climates. The range, which is shown as a dashed line in Fig. 4, indicated the evapotranspiration range from grassland to forest. The range of annual evapotranspiration in this study was almost within the range indicated by Zhang et al. (2001). In terms of the climatological aspect, the differences in the annual evapotranspiration in both forests and grasslands diminished with decreases in annual rainfall due to the strong suppression of the hydrological environment. This is because both forests and grasslands need to use water for evapotranspiration to maximize their photosynthesis production with limited water supplied as precipitation. Thus, it could be considered that the effect of the atmospheric situation (changes in T_a and/or D) on catchment water balance throughout the evapotranspiration processes is critical for low precipitation catchments, such as in northern Ukraine.

We constructed a time series of annual P_r , T_a , D , E and Q (Fig. 5). All annual variables showed an increasing trend with large fluctuation for each year. There was a significant increasing trend in annual T_a over the 25-year period (slope = $0.05 \text{ }^\circ\text{C year}^{-1}$, $p < 0.01$), but there were non-significant trends for other variables. Even D did not have significant long-term trend. Interestingly, the slight increase of P_r (2.7 mm year^{-1}) was not evenly divided into E and Q . The increasing slope of E (1.5 mm year^{-1}) was slightly larger than that of Q (1.3 mm year^{-1}). One reason may be that there was an uneven distribution of vegetation succession with no agricultural management (human pressure) in the CEZ (Yoschenko et al., 2019). However, it is also well known that the physical and biological drivers, such as vapor pressure deficit, soil moisture content and stomatal conductance, strongly control catchment scale evapotranspiration (e.g., Wilson and Baldocchi, 2000; Stoy et al., 2006; Igarashi et al., 2015a, 2015b). Thus, further analyses are needed to resolve the reasons for the long-term trend of water balance, especially allocation of P_r to E and Q with vegetation changes from field observations and vegetation dynamics models (see Sato et al., 2007).

Current and future climate water balance

We used a simple water balance model and have discussed the current water balance and its characteristics. In this section, the annual water balance of the study site in a future climate is shown. Fig. 6 illustrates the 20-year average for each hydrological component from current to most extreme future situation (RCP8.5 scenario). Bias-corrected future forcing data, such as P_r and D , increased with time, and changed significantly ($p < 0.05$, Tukey's test) from the current climate after 2040–2059 (Fig. 6 a and b). As the forcing data changed, the annual E also showed significant changes ($p < 0.05$, Tukey's test) (Fig. 6c), but the changes in annual Q were not clear (Fig. 7d). Based on the bias-corrected GCM results, it was predicted that the future annual P_r would be up to 1.24 times higher and future annual D also increased to 1.36 times higher compared with current levels. Our results showed that the water supply in the future will increase, but at the same time, the atmospheric situation will become drier, so the water supplied to the catchment will be consumed as evapotranspiration and will not lead to increasing river discharge.

The current and future seasonality of each variable is shown in Fig. 7. The ensemble monthly average over 20-year time series data showed a small increase in precipitation in winter and early summer (Fig. 7a). The ensemble monthly averaged air temperature also increased throughout the year, and the monthly air temperature was positive ($> 0 \text{ degC}$) in all months in the far future climate (2080–2099) (Fig. 7b). Increasing amounts of rainfall from November to March in future climates were remarkable (Fig. 7c). The relatively high air temperature and the chance of rainfall during the winter also led decreasing snowfall (Fig. 7d) and snow water equivalent (Fig. 7e). Monthly evapotranspiration also increased during the summer and beginning of autumn (June–September) (Fig. 7f). Interestingly, the increase in future air temperature was not enough to significantly increase winter and spring evapotranspiration via the vapor pressure deficit. It is important to note that an increase in future Q during the winter and spring (from January to April) is simulated, despite the decrease in snowfall and snow depth (Fig. 7g). Similar trends in seasonal dynamics were found in a study from a Polish-Russian river, and south Ukrainian river (Hesse et al., 2015) and Lithuanian river (Čerkasova et al., 2016) with increases to the river discharge in winter and decreases in spring as a result of temperature rises. Additionally, in some cases the maximum spring discharges will take place earlier. Didovets et al. (2017) indicated shifts in the seasonal distribution of runoff in Ukraine catchments. The spring high flow occurred earlier as a result of temperature increases and earlier snowmelt.

Consequently, the trend is an increase in river discharge in the winter season and a potential decrease in river discharge in the spring. They also showed that a potential reduction in discharge in spring was accompanied by a shift of the spring peak to earlier months under the projected future climate scenarios. In this study, it was considered that the warmer winter and spring temperature would decrease the snowfall, and increase the rainfall and, as a result, the peak of discharge shifted from April to March (Fig. 7g). The maximum daily discharge, which was formed by the spring snowmelt under the current climate, diminished under the future climate (Fig. 7h). In addition, a non-significant change in evapotranspiration from winter to spring was tightly coupled with winter discharge. From a climatology aspect, our study site could be classified as a relatively high atmospheric demand region (e.g., Budyko, 1961; Zhang et al., 2001). Approximately 84% of precipitation is consumed as evapotranspiration (Fig. 4). High evapotranspiration could directly influence the discharge rate throughout the soil water content. Thus, it could be considered that the combination of (1) increasing winter and spring rainfall, and (2) relatively little evapotranspiration, which enhanced the catchment scale water recharge in the soil moisture, gave rise to increased discharge during winter and spring. However, increasing precipitation during the summer months could not directly lead to increasing discharge because of the compensation effect of the relatively large evapotranspiration during the summer.

Implications for the future hydrological environment and radionuclide concentrations in Chernobyl rivers

At present, high levels of dissolved phase strontium-90 (^{90}Sr) are still being detected from the small catchment streams inside the CEZ. The main long-term source of exchangeable and available ^{90}Sr in the soils of CEZ is the gradually dissolving micron-size “fuel particles” accidentally released from the Chernobyl nuclear power plant Unit 4 (26/04/1986), formed by the mechanical destruction of nuclear fuel. It is well known that ^{90}Sr is one of the major high mobility radionuclides (Konoplev et al., 1992; Kashparov et al., 1999). During high flow events (e.g., snowmelt or heavy rainfall) ^{90}Sr is directly leached by surface runoff water from the contaminated surface soil and/or top layer of floodplain soils in the CEZ (e.g., Voitsekhovitch et al., 1993). This highly contaminated surface runoff enters streams and rivers leading to the increase of both the flow rate and ^{90}Sr concentration in river water system. Further studies conducted in the small watershed in the CEZ indicated that near-channel wetland areas can act as a source of ^{90}Sr for surface water. During the spring snowmelt and large rainfall events, the groundwater table in wetland areas rises, and these wetland areas then produce direct, more highly contaminated surface runoff to the river water system by the ‘saturation excess’ overland flow mechanism (Freed et al., 2003; 2004). Thus, increasing river discharge could play an important role in leaching radionuclides from the surface soil and transport to the river water system. Based on the simulated discharge time series, extreme value analysis of flood level was performed. Flood frequency curves of simulated discharge rates based on the Generalized Extreme Value (GEV) distribution (see more details in Intergovernmental Panel on Climate Change, 2001) were fitted to the annual maxima in the current (1999–2018) and far future (MRI-CGCM3 with RCP 8.5; 2080–2099) periods for the Sakhan catchment. The extreme river discharge was projected to decrease from 2.7 to 1.4 mm day⁻¹ in the 50-year extreme river discharge levels for the far future period compared to the current period (Fig. 8). Interestingly, it was shown that the future extreme river discharge will decrease compared to the current, although the decrease was not significant. The concentration of major radionuclides, such as ^{90}Sr (half-life = 28.8 years) and ^{137}Cs (half-life = 30.17 years), in the soil of Chernobyl catchments will continue to decrease into the future under the radioactive and environmental decay processes (e.g., Smith et al., 2000; Sasina et al., 2007). The diminishing of extreme river discharge from the hydrological projections could reduce the probability of high radionuclides concentrations in the river water system in the future. Thus, the trend of radionuclides concentration in the river water system will continue to decrease as predicted by the simple extrapolation of tendencies based on radioactive decay. Many other factors, such as chemical balance and resolution rate, contribute to the radionuclides concentrations in the river water system (Konoplev et al., 1992; Kashparov et al., 1999). Further hydro-chemical modeling will be needed for process-based understanding of radionuclides dynamics at the post-accident contaminated catchment.

Conclusion

This study focused on the catchment scale water balance at the Chernobyl Exclusion Zone in northern

Ukraine using a simple hydrological model. The model was validated with long-term discharge measurements from the radionuclides monitoring database and showed good agreement with observed data. Our results showed that 84% of annual input (sum of rainfall and snowmelt) was consumed as evapotranspiration, and discharge was estimated to be 16% under the current climate. We used bias-corrected future climate data for future water balance estimation at the study site in Chernobyl. In future climates, annual precipitation is expected to increase. However, the projected increase in the vapor pressure deficit led the consumption of precipitation as evapotranspiration and no significant increase in discharge. In this study, it was found that the warmer winter and spring temperature will decrease the snowfall and increase the rainfall. As a result, the peak discharge shifted from April to March. The increase in future Q during the winter and spring was formed by the combination of (1) increasing winter and spring rainfall, and (2) relatively low evapotranspiration, which enhanced the catchment scale water recharge in the soil moisture and gave rise to increased discharge during winter and spring. Stream discharge directly related to redistribution of radionuclides in the environment, thus it is considered that the implementation of this model could help with future water use and resources strategy and countermeasures for radionuclides in this region. Furthermore, the diminishing of extreme river discharge from the hydrological projections could reduce the probability of high radionuclides concentrations in the river water system in the future due to the reduction of surface runoff water from the contaminated surface soil and/or top layer of floodplain soils in the CEZ. The concentration of ^{90}Sr and ^{137}Cs in the soil of Chernobyl watersheds will continue to decrease in the future under the radioactive and environmental decay processes. As previous studies have shown, many factors, such as chemical balance and resolution rate, contribute to radionuclides concentrations in the river water system. Thus, further hydro-chemical modeling will be needed for process-based understanding of radionuclides dynamics at the post-accident contaminated catchment.

Acknowledgements

This work was supported by the Science and Technology Research Partnership for Sustainable Development JST-JICA, Japan (SATREPS project; PI. Kenji Nanba; JPMJSA1603). We thank Mr. Volodymyr Sarnavskiy, the staff of ECOCENTRE and UHMI in Ukraine for their assistance with fieldwork. We thank Leonie Seabrook, PhD, from Edanz Group (www.edanzediting.com/ac) for editing a draft of this manuscript.

Data availability statement

The data that support the findings of this study are available from the corresponding author upon reasonable request.

References

- Budyko MI. 1961. The Heat Balance of the Earth's Surface. *Soviet Geography* 2 (4): 3–13 DOI: 10.1080/00385417.1961.10770761
- Čerkasova N, Ertürk A, Zemlys P, Denisov V, Umgieser G. 2016. Curonian Lagoon drainage basin modelling and assessment of climate change impact. *Oceanologia* 58 (2): 90–102 DOI: 10.1016/j.oceano.2016.01.003
- Coles S. 2001. *An Introduction to Statistical Modeling of Extreme Values* (Intergovernmental Panel on Climate Change, ed.). Springer London: London. DOI: 10.1007/978-1-4471-3675-0
- Dai A. 2008. Temperature and pressure dependence of the rain-snow phase transition over land and ocean. *Geophysical Research Letters* 35 (12): 1–7 DOI: 10.1029/2008GL033295
- Didovets I, Lobanova A, Bronstert A, Snizhko S, Maule C, Krysanova V. 2017. Assessment of Climate Change Impacts on Water Resources in Three Representative Ukrainian Catchments Using Eco-Hydrological Modelling. *Water* 9 (3): 204 DOI: 10.3390/w9030204
- European Environment Agency. 2017. *Climate change, impacts and vulnerability in Europe 2016*. Luxembourg. DOI: 10.2800/534806

- Ewers BE, Oren R, Johnsen KH, Landsberg JJ. 2001. Estimating maximum mean canopy stomatal conductance for use in models. *Canadian Journal of Forest Research* 31 (2): 198–207 DOI: 10.1139/cjfr-31-2-198
- Farley KA, Jobbágy EG, Jackson RB. 2005. Effects of afforestation on water yield: A global synthesis with implications for policy. *Global Change Biology* 11 (10): 1565–1576 DOI: 10.1111/j.1365-2486.2005.01011.x
- Foley J a, Defries R, Asner GP, Barford C, Bonan G, Carpenter SR, Chapin FS, Coe MT, Daily GC, Gibbs HK, et al. 2005. Global consequences of land use. *Science* 309 (5734): 570–4 DOI: 10.1126/science.1111772
- Freed R, Smith L, Bugai D. 2004. The effective source area of 90Sr for a stream near Chernobyl, Ukraine. *Journal of Contaminant Hydrology* 71 (1–4): 1–26 DOI: 10.1016/j.jconhyd.2003.07.002
- Freed R, Smith L, Bugai D. 2003. Seasonal Changes of the 90 Sr Flux in the Borschi Stream , Chernobyl. *Environmental Science and Pollution Research* 1 (1): 48–56
- Garcia-Sanchez L, Konoplev A, Bulgakov A. 2005. Radionuclide entrainment coefficients by wash-off derived from plot experiments near Chernobyl. *Radioprotection* 40 (September): S519–S524 DOI: 10.1051/radiopro:2005s1-076
- Garcia-Sanchez L, Konoplev A V. 2009. Watershed wash-off of atmospherically deposited radionuclides: A review of normalized entrainment coefficients. *Journal of Environmental Radioactivity* 100 (9): 774–778 DOI: 10.1016/j.jenvrad.2008.08.005
- Gollan T, Turner NC, Schulze E-D. 1985. The responses of stomata and leaf gas exchange to vapour pressure deficits and soil water content. *Oecologia* 65 (3): 356–362 DOI: 10.1007/bf00378909
- Graham LP, Andréasson J, Carlsson B. 2007. Assessing climate change impacts on hydrology from an ensemble of regional climate models, model scales and linking methods - A case study on the Lule River basin. *Climatic Change* 81 (SUPPL. 1): 293–307 DOI: 10.1007/s10584-006-9215-2
- Hesse C, Stefanova A, Krysanova V. 2015. Comparison of water flows in four European lagoon catchments under a set of future climate scenarios. *Water (Switzerland)* 7 (2): 716–746 DOI: 10.3390/w7020716
- Hesse C, Stefanova A, Krysanova V. 2015. Comparison of water flows in four European lagoon catchments under a set of future climate scenarios. *Water (Switzerland)* 7 (2): 716–746 DOI: 10.3390/w7020716
- Hock R. 2003. Temperature index melt modelling in mountain areas. *Journal of Hydrology* 282 (1–4): 104–115 DOI: 10.1016/S0022-1694(03)00257-9
- Igarashi Y, Katul GG, Kumagai T, Yoshifuji N, Sato T, Tanaka N, Tanaka K, Fujinami H, Suzuki M, Tantasirin C. 2015. Separating physical and biological controls on long-term evapotranspiration fluctuations in a tropical deciduous forest subjected to monsoonal rainfall. *Journal of Geophysical Research: Biogeosciences* 120 (7): 1262–1278 DOI: 10.1002/2014JG002767
- Igarashi Y, Kumagai T, Yoshifuji N, Sato T, Tanaka N, Tanaka K, Suzuki M, Tantasirin C. 2015. Environmental control of canopy stomatal conductance in a tropical deciduous forest in northern Thailand. *Agricultural and Forest Meteorology* 202: 1–10 DOI: 10.1016/j.agrformet.2014.11.013
- International Atomic Energy Agency. 2006. Radiological Conditions in the Dnieper River Basin
- Jacob D, Petersen J, Eggert B, Alias A, Christensen OB, Bouwer LM, Braun A, Colette A, Déqué M, Georgievski G, et al. 2014. EURO-CORDEX: New high-resolution climate change projections for European impact research. *Regional Environmental Change* 14 (2): 563–578 DOI: 10.1007/s10113-013-0499-2
- Jasechko S, Sharp ZD, Gibson JJ, Birks SJ, Yi Y, Fawcett PJ. 2013. Terrestrial water fluxes dominated by transpiration. *Nature* 496 (7445): 347–350 DOI: 10.1038/nature11983
- Joseph JF, Guillaume JHA. 2013. Using a parallelized MCMC algorithm in R to identify appropriate likelihood functions for SWAT. *Environmental Modelling & Software* 46: 292–298 DOI: 10.1016/j.envsoft.2013.03.012

Kashparov VA, Oughton DH, Zvarich SI, Protsak VP, Levchuk SE. 1999. Kinetics of fuel particle weathering and ^{90}Sr mobility in the Chernobyl 30-km exclusion zone. *Health Physics* 76 (3): 251–259 DOI: 10.1097/00004032-199903000-00006

Kjellström E, Nikulin G, Hansson U, Strandberg G, Ullerstig A. 2011. 21st century changes in the European climate: uncertainties derived from an ensemble of regional climate model simulations. *Tellus A: Dynamic Meteorology and Oceanography* 63 (1): 24–40 DOI: 10.1111/j.1600-0870.2010.00475.x

Konoplev A V, Bulgakov AA, Popov VE, Bobovnikova TI. 1992. Behaviour of long-lived Chernobyl radionuclides in a soil-water system. *Analyst* 117 (6): 1041–1047 DOI: 10.1039/an9921701041

Kumagai T, Katul GG, Saitoh TM, Sato Y, Manfroi OJ, Morooka T, Ichie T, Kuraji K, Suzuki M, Porporato A. 2004. Water cycling in a Bornean tropical rain forest under current and projected precipitation scenarios. *Water Resources Research* 40 (1) DOI: 10.1029/2003WR002226

Laio F, Porporato A, Ridolfi L, Rodriguez-Iturbe I. 2001. Plants in water-controlled ecosystems: active role in hydrologic processes and response to water stress: II. Probabilistic soil moisture dynamics. *Advances in Water Resources* 24 (7): 707–723 DOI: 10.1016/S0309-1708(01)00005-7

Lehner B, Döll P, Alcamo J, Henrichs T, Kaspar F. 2006. Estimating the Impact of Global Change on Flood and Drought Risks in Europe: A Continental, Integrated Analysis. *Climatic Change* 75 (3): 273–299 DOI: 10.1007/s10584-006-6338-4

Manzoni S, Vico G, Katul G, Fay P a., Polley W, Palmroth S, Porporato A. 2011. Optimizing stomatal conductance for maximum carbon gain under water stress: A meta-analysis across plant functional types and climates. *Functional Ecology* 25 (3): 456–467 DOI: 10.1111/j.1365-2435.2010.01822.x

Nash JE, Sutcliffe JV. 1970. River flow forecasting through conceptual models part I — A discussion of principles. *Journal of Hydrology* 10 (3): 282–290 DOI: 10.1016/0022-1694(70)90255-6

Nepyvoda V. 2005. Forestry in the chornobyl exclusion zone: Wrestling with an invisible rival. *Journal of Forestry* 103 (1): 36–40 DOI: 10.1093/jof/103.1.36

Palmroth S, Katul GG, Hui D, McCarthy HR, Jackson RB, Oren R. 2010. Estimation of long-term basin scale evapotranspiration from streamflow time series. *Water Resources Research* 46 (10): 1–13 DOI: 10.1029/2009WR008838

Pataki DE, Oren R. 2003. Species differences in stomatal control of water loss at the canopy scale in a mature bottomland deciduous forest. *Advances in Water Resources* 26 (12): 1267–1278 DOI: 10.1016/j.advwatres.2003.08.001

Piniewski M, Szczesniak M, Huang S, Kundzewicz ZW. 2018. Projections of runoff in the Vistula and the Odra river basins with the help of the SWAT model. *Hydrology Research* 49 (2): 303–317 DOI: 10.2166/nh.2017.280

Sasina NV, Smith JT, Kudelsky AV, Wright SM. 2007. “Blind” testing of models for predicting the ^{90}Sr activity concentration in river systems using post-Chernobyl monitoring data. *Journal of Environmental Radioactivity* 92 (2): 63–71 DOI: 10.1016/j.jenvrad.2006.09.007

Sato H, Itoh A, Kohyama T. 2007. SEIB-DGVM: A new Dynamic Global Vegetation Model using a spatially explicit individual-based approach. *Ecological Modelling* 200: 279–307 DOI: 10.1016/j.ecolmodel.2006.09.006

Smith JT, Belova N V, Bulgakov AA, Comans RNJ, Konoplev A V, Kudelsky A V, Madruga MJ, Voitsek-hovitch O V, Zibold G. 2005. The “AQUASCOPE” simplified model for predicting SIMPLIFIED MODEL FOR PREDICTING ^{89}Sr , ^{90}Sr , ^{131}I , and $^{134,137}\text{Cs}$ In surface water s after a laege-scale radioactive fallout. *Health Physics* 89 (6): 628–644 DOI: 10.1097/01.HP.0000176797.66673.b7

Smith JT, Comans RN, Beresford N a, Wright SM, Howard BJ, Camplin WC. 2000. Chernobyl’s legacy in food and water. *Nature* 405 (May): 141 DOI: 10.1038/35012139

Sperna Weiland FC, Van Beek LPH, Kwadijk JCJ, Bierkens MFP. 2010. The ability of a GCM-forced hydrological model to reproduce global discharge variability. *Hydrology and Earth System Sciences* 14 (8): 1595–1621 DOI: 10.5194/hess-14-1595-2010

Stoy PC, Katul GG, Siqueira MBS, Juang J-Y, Novick KA, McCarthy HR, Christopher Ooshi A, Uebelherr JM, Kim H-S, Oren R. 2006. Separating the effects of climate and vegetation on evapotranspiration along a successional chronosequence in the southeastern US. *Global Change Biology* 12 (11): 2115–2135 DOI: 10.1111/j.1365-2486.2006.01244.x

Tsuji H, Nishikiori T, Yasutaka T, Watanabe M, Ito S, Hayashi S. 2016. Behavior of dissolved radiocesium in river water in a forested watershed in Fukushima Prefecture. *Journal of Geophysical Research: Biogeosciences* 121 (10): 2588–2599 DOI: 10.1002/2016JG003428

UNSCEAR (2000) Report to the General Assembly: Sources and effects of ionizing radiation. Volume II, Annex J. United Nations, New York, pp. 453–551.

Voitsekhevitch O, Kanivets V, Laptev G, Biley L. 1993. Hydrological Processes and their influence on radionuclide behaviour and transport by surface water pathways as applied to water protection after Chernobyl accident. In *Hydrological Considerations In Relation to Nuclear Power Plants UNESCO CHERNOBYL PROGRAMME*: Paris, France; 83–105.

Vrugt JA, Ter Braak CJF, Diks CGH, Robinson BA, Hyman JM, Higdon D. 2009. Accelerating Markov chain Monte Carlo simulation by differential evolution with self-adaptive randomized subspace sampling. *International Journal of Nonlinear Sciences and Numerical Simulation* 10 (3): 273–290 DOI: 10.1515/IJNSNS.2009.10.3.273

Wakiyama Y, Onda Y, Yoshimura K, Igarashi Y, Kato H. 2019. Land use types control solid wash-off rate and entrainment coefficient of Fukushima-derived ¹³⁷Cs, and their time dependence. *Journal of Environmental Radioactivity* (October 2017): 105990 DOI: 10.1016/j.jenvrad.2019.105990

Watanabe S, Kanae S, Seto S, Yeh P-J-F, Hirabayashi Y, Oki T. 2012. Intercomparison of bias-correction methods for monthly temperature and precipitation simulated by multiple climate models. *Journal of Geophysical Research* 117 (D23): D23114 DOI: 10.1029/2012JD018192

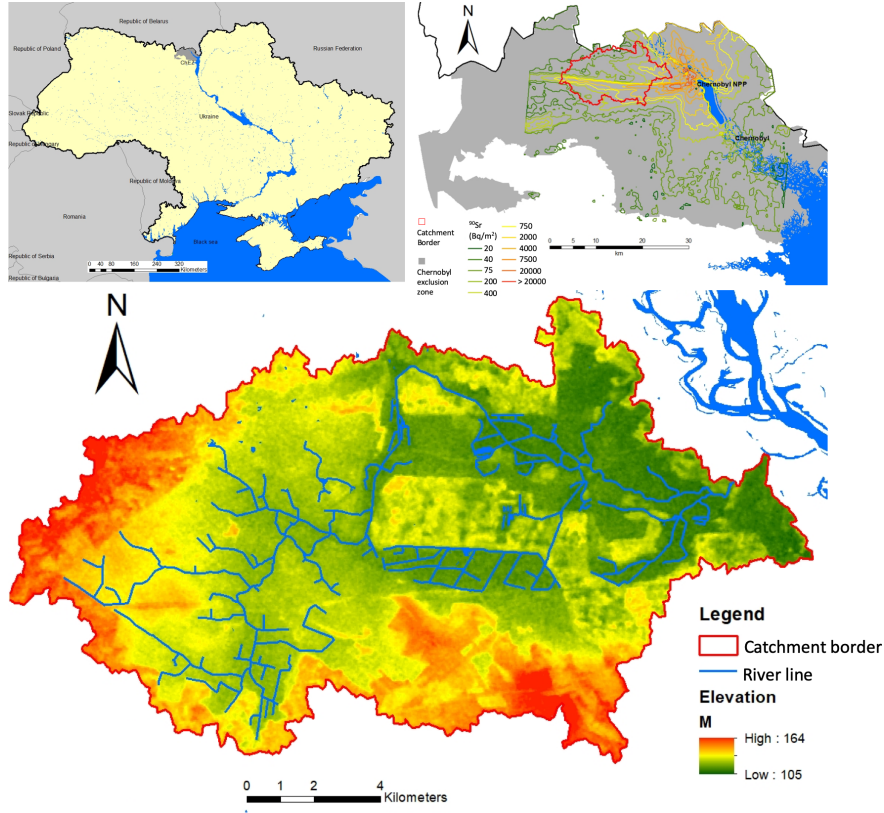
Wilson KB, Baldocchi DD. 2000. Seasonal and interannual variability of energy fluxes over a broadleaved temperate deciduous forest in North America. *Agricultural and Forest Meteorology* 100: 1–18 DOI: 10.1016/S0168-1923(99)00088-X

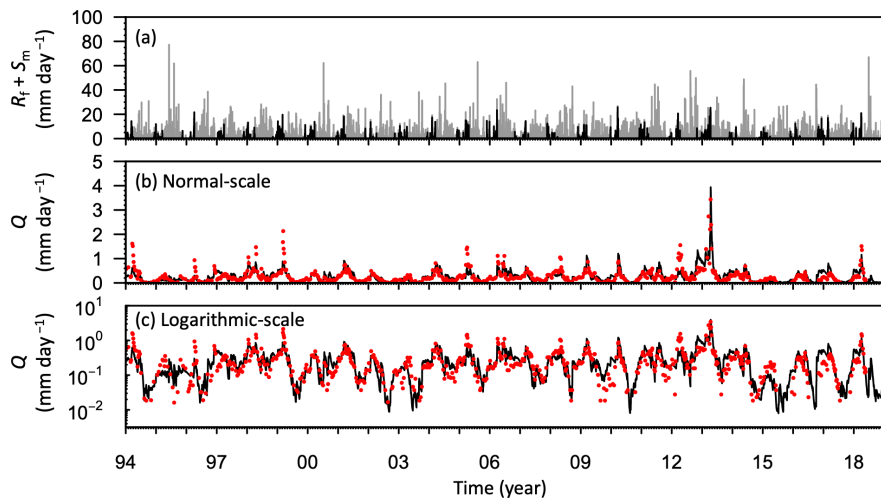
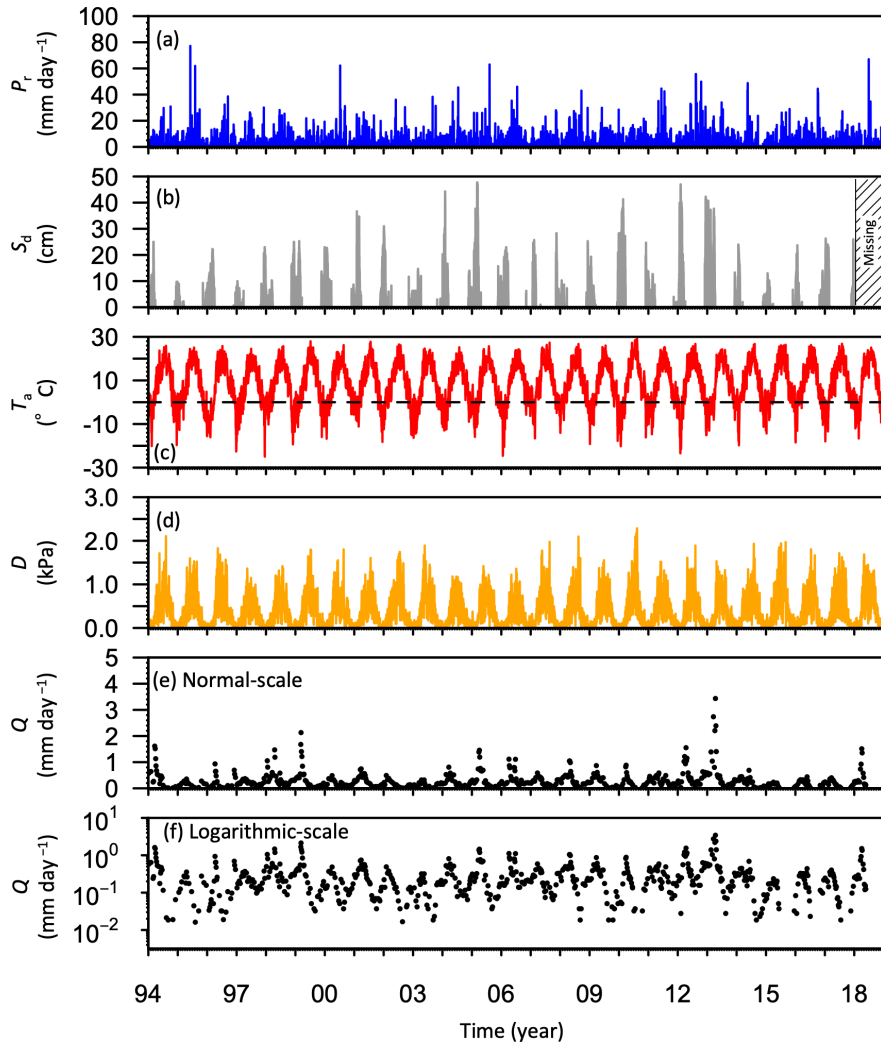
Yoschenko V, Kashparov V, Ohkubo T. 2019. Radioactive Contamination in Forest by the Accident of Fukushima Daiichi Nuclear Power Plant: Comparison with Chernobyl. In *Radiocesium Dynamics in a Japanese Forest Ecosystem* Springer Singapore: Singapore; 3–22. DOI: 10.1007/978-981-13-8606-0_1

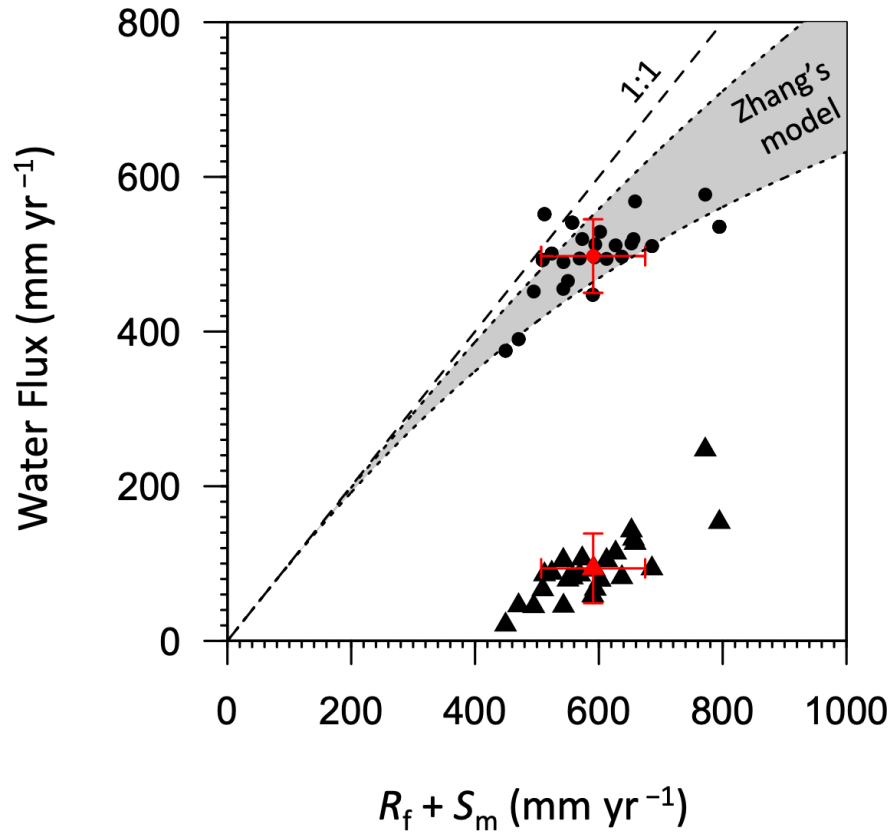
Yoshimura K, Onda Y, Sakaguchi A, Yamamoto M, Matsuura Y. 2015. An extensive study of the concentrations of particulate/dissolved radiocaesium derived from the Fukushima Dai-ichi Nuclear Power Plant accident in various river systems and their relationship with catchment inventory. *Journal of Environmental Radioactivity* 139: 370–378 DOI: 10.1016/j.jenvrad.2014.08.021

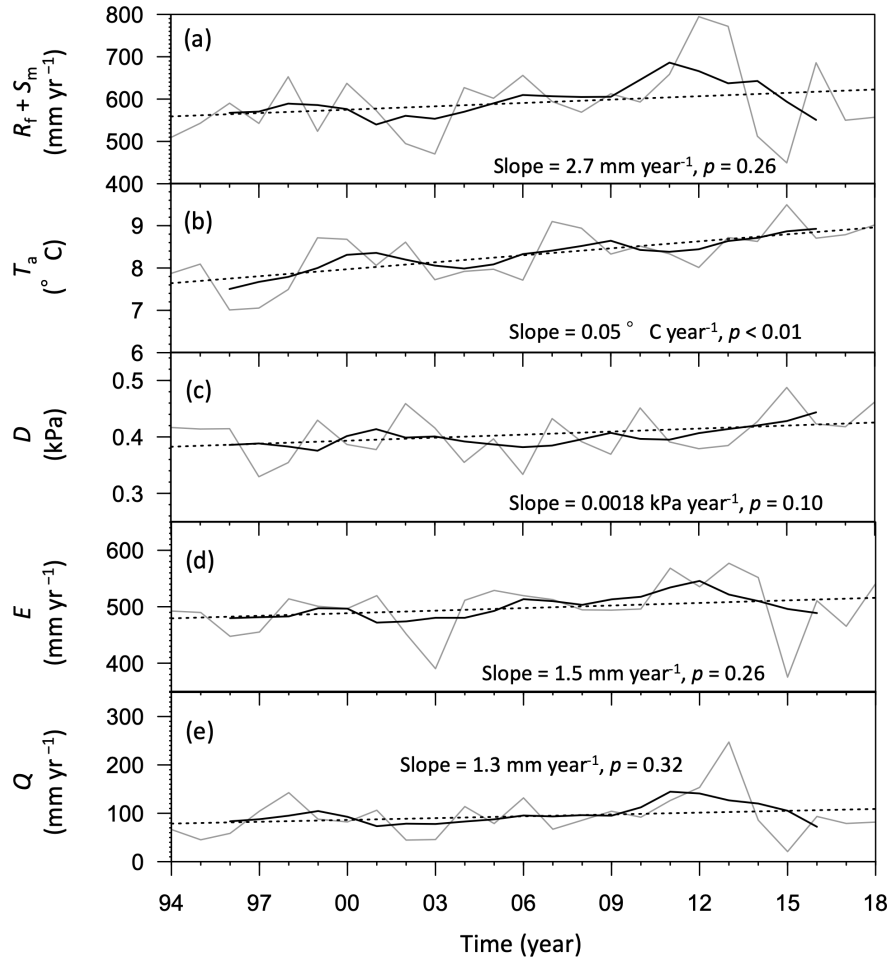
Yukimoto S, Adachi Y, Hosaka M, Sakami T, Yoshimura H, Hirabara M, Tanaka TY, Shindo E, Tsujino H, Deushi M, et al. 2012. A new global climate model of the Meteorological Research Institute: MRI-CGCM3: -Model description and basic performance-. *Journal of the Meteorological Society of Japan* 90 (A): 23–64 DOI: 10.2151/jmsj.2012-A02

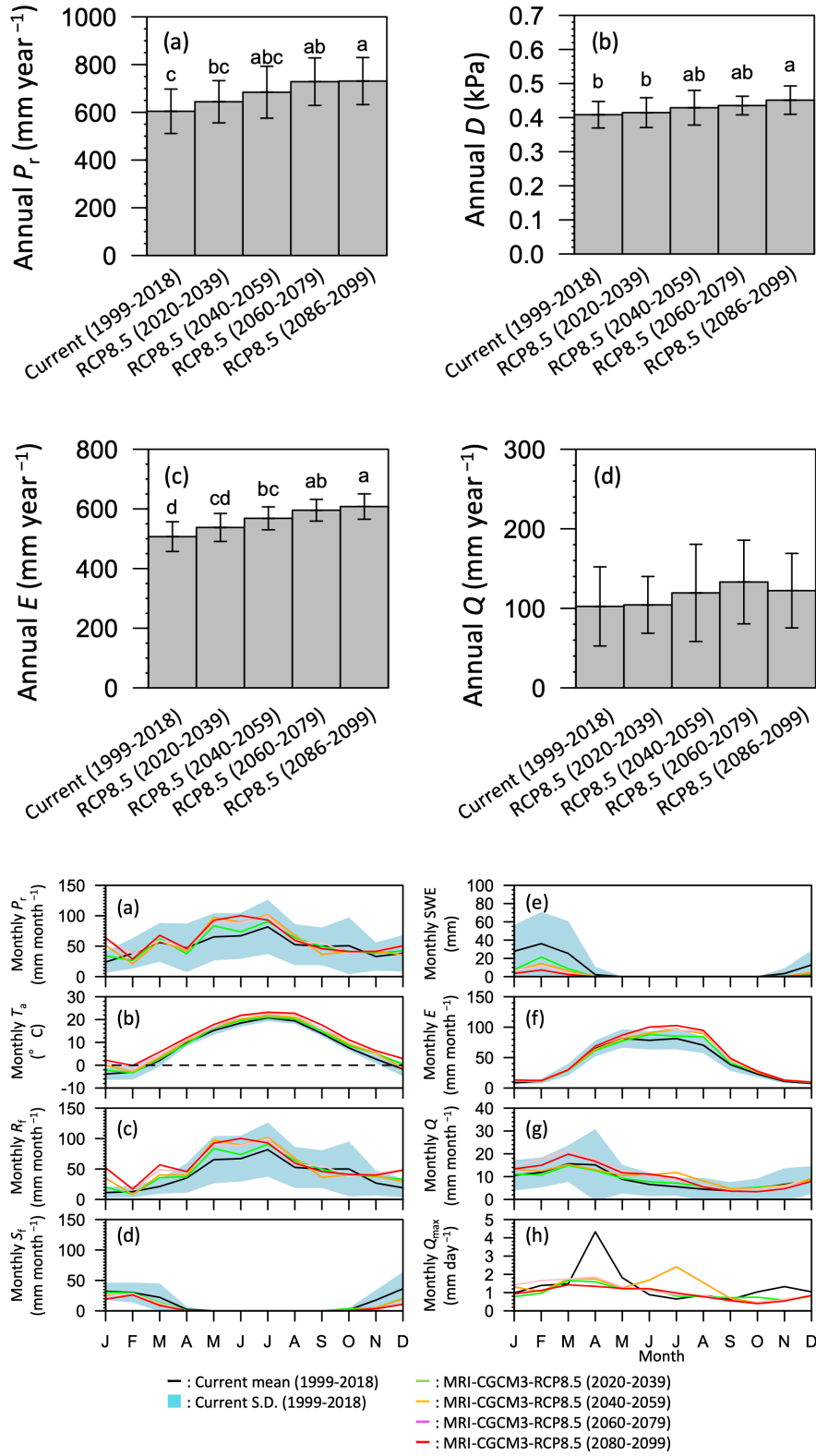
Zhang L, Dawes WR, Walker GR. 2001. Response of mean annual evapotranspiration to vegetation changes at catchment scale. *Water Resources Research* 37 (3): 701–708 DOI: 10.1029/2000WR900325

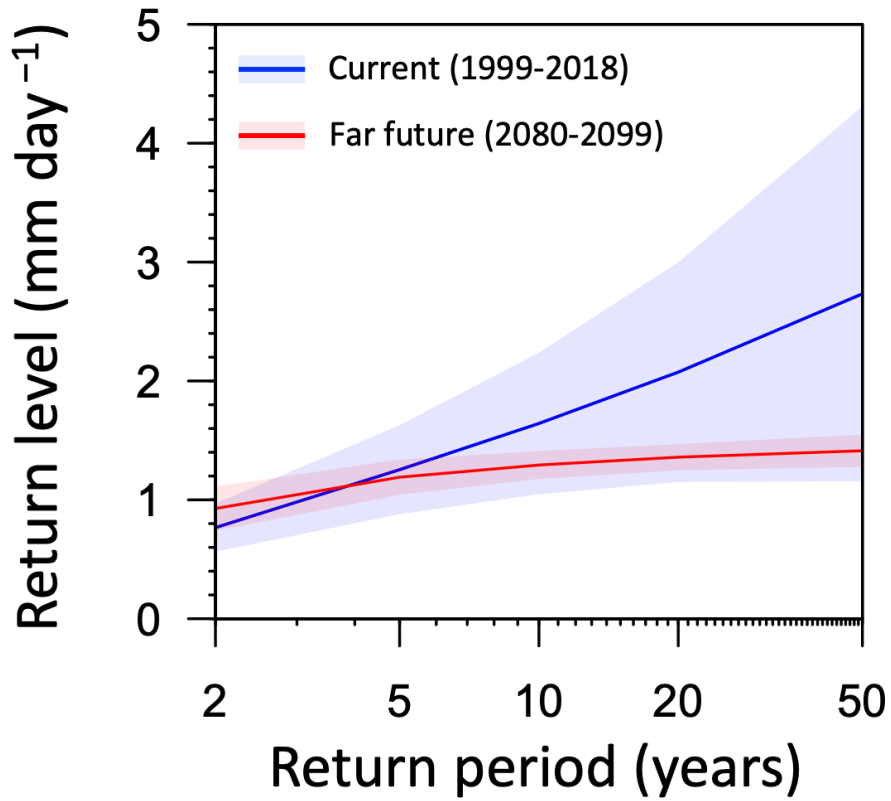












Model	Abbreviation	Units	Definition
Hydrologic Model	P_r	mm	Precipitation
	R_f	mm	Rainfall
	W	mm	Soil water content
	E	mm	Catchment scale evapotranspiration
	Q	mm	Discharge
	T_s	° C	Surface air temperature
	D	kPa	Vapor pressure deficit
	W_{max}	mm	Maximum water depth
	Q_o	mm day ⁻¹	Maximum run-off flux parameter
	m	unitless	Model parameter (equation 2)
	E_w	mm day ⁻¹	Soil evaporation
	E_{max}	mm day ⁻¹	Maximum transpiration
	α	kPa ⁻¹	Unit conversion factor
	θ	unitless	soil moisture content
	θ_h	unitless	soil moisture content at the hygroscopic point
	θ_w	unitless	soil moisture content at the plant wilting point
	θ^*	unitless	psoil moisture content at the plant stress point
	Q_{max}	mm day ⁻¹	Daily maximum discharge
Snow model	S	mm	Snow water equivalent
	SF	mm day ⁻¹	Snowfall in water equivalent
	SM	mm day ⁻¹	Snowmelt in water equivalent
	a	-	Model parameter (equation 7; = -48.2292; Dai et al., 2008)
	b	-	Parameter of temperature dependence of snow frequency model (= 0.7205; Dai et al., 2008)
	c	-	Parameter of temperature dependence of snow frequency model (= 1.1662; Dai et al., 2008)
	d	-	Parameter of temperature dependence of snow frequency model (= 1.0223; Dai et al., 2008)
	f_m	mm ° C ⁻¹ day ⁻¹	melt factor in degree-day approach in Hock (2003)

	Symbol	Value
Model parameters	W_{\max} (mm)	675
	Q_o (mm day ⁻¹)	14.3
	m (unitless)	3.8
	E_w (mm day ⁻¹)	2.20
	E_{\max} (mm day ⁻¹)	4.84
Agreement	Nash-Sutcliffe	0.62
	R^2	0.79

	Precipitation (mm year ⁻¹)	Evapotranspiration (mm year ⁻¹)	Discharge (mm year ⁻¹)
Average	604	507	102
SD	93	50	50